Weierstraß–Institut
für Angewandte Analysis und Stochastik

im Forschungsverbund Berlin e.V.

Preprint ISSN 0946 – 8633

Excitability of a DFB laser with short external cavity

Mindaugas Radziunas [1,2] , Hans-Jürgen Wünsche[2] , Olaf Brox[3] ,

Fritz Henneberger[2]

submitted: 29 Jan 2002

1 Weierstraß-Insitute für
Angewandte Analysis und Stochastik,
Mohrenstr. 39,
10117 Berlin, Germany
E-Mail: radziuna@wias-berlin.de

2 Humboldt-Universität zu Berlin,
Institut für Physik,
Invalidenstr. 110,
10115 Berlin, Germany
E-Mail: wuensche@physik.hu-berlin.de
E-mail: henne@physik.hu-berlin.de

3 Heinrich-Hertz-Institut für
Nachrichtentechnik Berlin GmbH,
Einsteinufer 37,
10587 Berlin, Germany
E-mail: brox@hhi.de

Preprint No. 712

Berlin 2002

1991 *Mathematics Subject Classification.* 78A60,78-05,35P10.

Key words and phrases. DFB laser, excitability, modes, traveling wave equations.

Edited by
Weierstraß–Institut für Angewandte Analysis und Stochastik (WIAS)
Mohrenstraße 39
D — 10117 Berlin
Germany

Fax: + 49 30 2044975
E-Mail (X.400): c=de;a=d400-gw;p=WIAS-BERLIN;s=preprint
E-Mail (Internet): preprint@wias-berlin.de
World Wide Web: http://www.wias-berlin.de/

Abstract

We discuss some aspects of the excitability in a semiconductor laser with short external cavity. It is demonstrated both theoretically and experimentally how a two-section semiconductor laser consisting of a DFB section and an integrated passive phase tuning section performs an excitable response to optical injection. A mode analysis of the model equations allows to understand and explain the origin of the excitability.

1 Introduction

The notion of excitability originally comes from biology [1, 2, 3] and chemistry [4]. By definition used in neurobiology [5, 6], an excitable system should exhibit the following features: i) existence of a threshold perturbation, above which the large response appears, ii) weak dependence of the response on the magnitude of the perturbation above and below threshold.

Recently excitability has been discussed also in optical systems such as cavities [7], lasers with a saturable absorber [8], semiconductor lasers subjected to delayed optical feedback [9, 10], optical injection [11] or lasers with a short external cavity [12, 13]. We focus on a more detailed theoretical analysis of the excitability reported in [13].

Theoretical works discussing excitability in the laser models have been followed only by few experimental works, where the observation of excitability of power dropouts in the low-frequency fluctuation regime of a laser diode with external feedback is still under debate [14, 15, 16, 17, 18]. Therefore, in the present study we pay similar attention to the theoretical discussion as well as to the experimental verification of the predicted effects.

We consider a two-section semiconductor laser consisting of a DFB section and an integrated passive phase tuning section having similar length with a cleaved facet as end mirror. Such a laser is represented schematically in Fig. 1. The section with 1.3 micron gap wavelength does not couple to the laser radiation but carrier injection enables to change its refractive index and so to tune the optical phase fed back into the active region.

In contrast to the laser with distant external feedback, the considered laser design allows to achieve an excellent mode control. A bifurcation analysis shows the ultimate hop between two compound cavity modes within every phase cycle. This transition of the modes is also associated with a two-mode homoclinic bifurcation close to

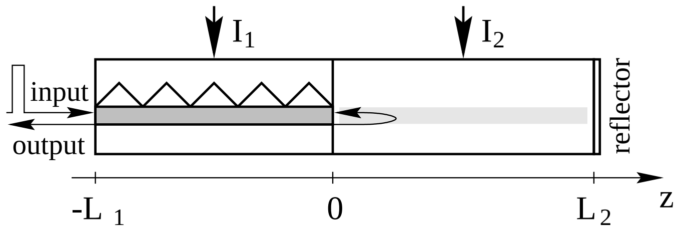

Figure 1: *Scheme of a DFB laser with integrated short external cavity.*

which the system becomes excitable. Such excitability is clearly demonstrated in the experimental response to optical injection comparing well with calculations.

The paper is organised as follows. We present the model equations in Section 2. In Section 3 we define the notion of carrier dependent optical modes and demonstrate theoretically and experimentally switching between different mode solutions when tuning the field feedback phase parameter. In Section 4 we determine the feedback phase conditions where excitability can be observed. Section 5 discusses mode decomposition of optical fields. Two modes governing the laser response to the super-threshold perturbation are indicated. The phase portrait of the excitable system is given in Section 6. The influence of nearby in the parameter space existing homoclinic bifurcation and possible multi-pulse response to perturbation is discussed. Finally, some conclusions are given in Section 7.

2 Model of two section DFB laser

The DFB laser with integrated short external cavity consists of an highly pumped active DFB section with the length $L_1 = 200$ μm (interval $z \in [-L_1, 0]$ in Fig. 1), and passive integrated external cavity section with the length $L_2 = 200$ μm (interval $z \in [0, L_2]$ in the same figure).

To model the behaviour of optical fields $\psi(z,t) = (\psi^+, \psi^-)^T$, polarisation functions $p(z,t) = (p^+, p^-)^T$ within all laser device $z \in [-L_1, L_2]$ and mean carrier density $n(t)$ within an active DFB section we use the Travelling Wave equation model (see [19]):

$$\begin{aligned}
\frac{-i}{v_{gr}}\frac{\partial}{\partial t}\psi^{\pm}(z,t) &= \Big(\pm i\frac{\partial}{\partial z} - \Big(\beta(z,n(t)) - \frac{i\alpha}{2}\Big)\Big)\psi^{\pm} - \kappa\psi^{\mp} + \frac{ig_P}{2}(\psi^{\pm} - p^{\pm}); \\
-i\frac{\partial}{\partial t}p^{\pm}(z,t) &= -i\gamma_P(\psi^{\pm} - p^{\pm}) + \omega_P p^{\pm}; \\
\frac{d}{dt}n(t) &= \frac{I_1}{eV_1} - (An + Bn^2 + Cn^3) - v_{gr}\Im m(\psi, 2\beta\psi - ig_P(\psi - p))_1; \\
\textit{b.c.}\;\; \psi^+(-L_1,t) &= r_1\psi^-(-L_1,t) + a_{inp}(t)e^{i\omega_{inp}t}, \quad \psi^-(L_2,t) = r_2\psi^+(L_2,t). \qquad (1)
\end{aligned}$$

The laser parameters are similar to those discussed in [13]. The real coefficients α and κ are given separately for each section and describe internal loses and field coupling due to the Bragg gratings. In our case we use $\alpha_1 = 25$ cm^{-1}, $\alpha_2 = 20$ cm^{-1}, $\kappa_1 = 180$ cm^{-1} and $\kappa_2 = 0$. Polarisation parameters g_P, γ_P and ω_P allow to approximate gain dispersion with a Lorentzian function, indicating height, half width at the half maximum and central frequency of this function respectively. We assume $g_{P,1} = 100$ cm^{-1}, $\gamma_{P,1} \sim 30$ nm, $\omega_{P,1} \sim 3$ nm and $g_{P,2} = 0$.

The propagation constant $\beta(z,t)$ in different sections is given by

$$\beta(z,t) = \begin{cases} \beta_1 = \delta_1 + g'\Gamma(i+\alpha_H)(n(t)-n_{tr})/2, & \text{if} \quad z \in [-L_1, 0] \\ \beta_2 = \delta_2 = 2\pi\varphi/(2L_2), & \text{if} \quad z \in [0, L_2] \end{cases} . \tag{2}$$

Here $\alpha_H = -5$, $g = 2 \cdot 10^{-17}$ cm^{-1}, $\Gamma = 0.3$, $n_{tr} = 10^{-18}$ cm^{-3} are linewidth enhancement factor, differential gain, confinement factor and transparency carrier density in the active section respectively. The parameters $\delta_1 \sim 2.2$ nm and δ_2 indicate the detuning from the reference frequency. Parameter φ defined in the formula above indicate a phase change of the forward propagating field and reflected back from the facet $z = L_1$ field at the junction $z = 0$.

The constants $I_1 = 50$ mA and I_2 represent current injection into DFB section and are the control parameters available in experiments. In modelling, we fix the first current and model impact of the second current by tuning parameter φ (see corresponding discussion in [20]).

The constants $V_1 = L_1 \cdot 0.15$ μm $\cdot 3$ μm, $A = 3 \cdot 10^8$ s, $B = 1 \cdot 10^{-16}$ s$\cdot$m^3, $C = 1 \cdot 10^{-40}$ s$\cdot$m^6 give volume of the active zone of DFB section and three recombination coefficients respectively. An expression $(\xi,\eta)_1$ shows an average of the complex function $\xi^{*T}(z)\eta(z)$ over the active DFB section:

$$(\xi,\eta)_1 = \frac{1}{L_1}\int_{-L_1}^{0} \xi^{+*}\eta^{+} + \xi^{-*}\eta^{-}\, dz.$$

Thus, after a proper normalisation of the fields $\psi(z,t)$, $(\psi,\psi)_1$ gives the mean photon density within DFB section.

We have also used field reflectivity coefficients $r_1 = 0$ and $r_2 = \sqrt{0.3}$. A positive function $a_{inp(t)}$ entering boundary conditions in 1 allow to model an injection of a short optical pulse at the frequency ω_{inp}. Finally, the parameters e and $v_{gr} = c_0/3.4$ are electron charge and group velocity respectively.

3 Dynamics of the laser for different phase of optical feedback

Let us assume at the beginning, that we have no external signal, i.e., the function $a(t)$ entering the boundary conditions of 1 is equal to zero. Different solutions of TWE model 1 after some transient time are attracted by some solution located on the invariant manifold of the state space. In the sequel we shall refer to stable (or unstable) solution supposing that it is located exactly on such stable (or unstable) invariant manifold.

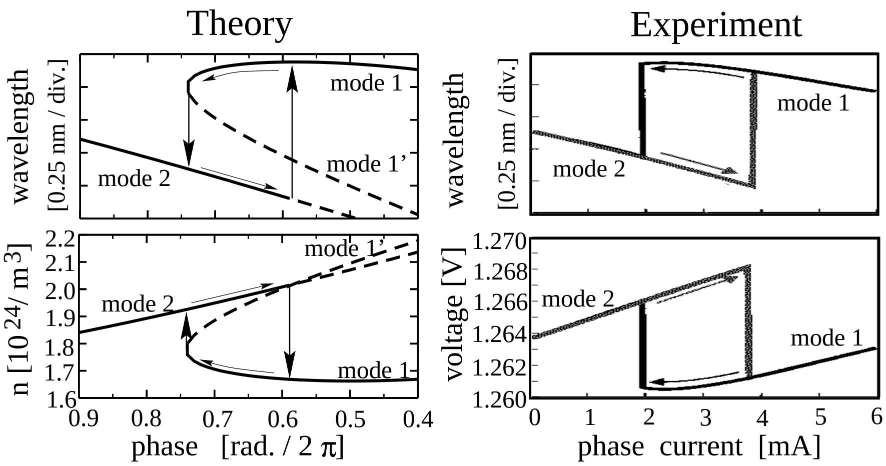

Figure 2: *Left: theoretical predictions. Right: experimental results. Solid and dashed thick lines show stable und unstable stationary solutions. Upper diagrams: lasing wavelengths of the stationary states. Lower diagrams: threshold carrier density (theory) and applied voltage (experiments). Bistability is observed in the interval* $[B, F]$.

Tuning the phase parameter φ in our model or the current injection into the phase tuning section for similar lasers in experiments we can observe transitions between such solutions (see [21]). Stable solutions can be observed when integrating model equations 1 or making experiments. Fig. 2 shows such transitions between stationary states caused by the changes of parameters. Solid lines in the left and right parts of this figure represent results of integration of model equations and measurements respectively. Here upper figures show computed or measured wavelength of the stationary lasing state, while lower figures represent computed carrier density in theory or applied voltage in experiments.

In both cases one can see hysteresis of the solution, that is, the dependence of the lasing state on the direction of parameter variation. As we have seen after more detailed study of the model equations 1, transition from the state 1 to the state 2 at $\varphi = B$ is due to saddle node bifurcation of the stationary state 1, while at $\varphi = E$ the stable stationary state 2 loses its stability in the Hopf bifurcation, the resulting high frequency stable limit cycle (first discussed theoretically for similar lasers in [22]) short afterwards at $\varphi = F$ loses its stability in the torus bifurcation and the system approaches the only remaining stable stationary state 1.

The dashed lines in the left part of Fig. 2 show unstable stationary states. The detection of unstable solutions, in general, is not possible in experiments and requires more advanced technique in modelling. In order to find all stationary (possibly unstable) solutions we can exploit the notion of carrier dependent modes (see [23]).

For this reason we write the optical field and polarisation equations in 1 in operator form:

$$-i\frac{\partial}{\partial t}\begin{pmatrix}\psi\\ p\end{pmatrix} = H(n)\begin{pmatrix}\psi\\ p\end{pmatrix}. \tag{3}$$

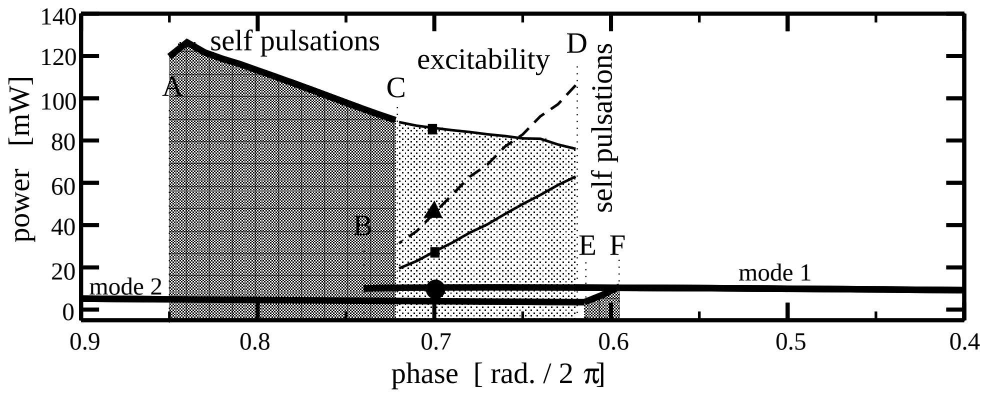

Figure 3: *Solid thick lines show stable stationary solutions or maximal value of stable self pulsating solution. Thin solid and dashed lines show strength of threshold injection and response of the system just before and after threshold perturbation. Intensively and light shadowed areas indicate regions where stable self pulsations and excitability can be observed, respectively.*

Here an operator H is dependent on the slowly varying carrier density n. The normalized carrier dependent modes

$$(\Theta_j(z,n), \Omega_j(n)), \qquad \text{where} \qquad \Theta_j = \begin{pmatrix} \Phi_j \\ \Pi_j \end{pmatrix}, \quad \Phi_j = \begin{pmatrix} \Phi_j^+ \\ \Phi_j^- \end{pmatrix}, \quad \Pi_j = \begin{pmatrix} \Pi_j^+ \\ \Pi_j^- \end{pmatrix},$$

solve the eigenvalue equation

$$\begin{array}{ll} \Omega_j(n)\Theta_j(z,n) = H(n)\Theta_j(z,n), & \Phi_j^-(-L_1,n) = 1, \\ \Phi_j^+(-L_1,n) = r_1\Phi_j^-(-L_1,n), & \Phi_j^-(L_2,n) = r_2\Phi_j^+(L_2,n). \end{array} \tag{4}$$

Let us assume that the positive constants $\bar{n}$ and $\bar{f}_j$ satisfy the relations

$$\Im m(\Omega_j(\bar{n})) = 0, \qquad \bar{f}_j^2 = \frac{I_1/(eV_1) - (A\bar{n} + B\bar{n}^2 + C\bar{n}^3)}{v_{gr}(\Phi_j(\bar{n}), \Phi_j(\bar{n}))_1 \left(2\Im m\beta_1(\bar{n}) - g_P \frac{(\omega_P - \Omega_j(\bar{n}))^2}{(\omega_P - \Omega_j(\bar{n}))^2 + \gamma_P^2}\right)}.$$

Then these constants define the stationary (rotational wave) solution of 1

$$n(t) = \bar{n}, \qquad \begin{pmatrix} \psi \\ p \end{pmatrix} = \bar{f}_j e^{i\phi_j}\Theta_j(z,\bar{n})e^{i\Omega_j(\bar{n}_j)t}, \qquad \phi_j \in [0, 2\pi],$$

with optical frequency and output power at the left facet determined by $\Re e(\Omega_j(\bar{n}))$ and $\bar{f}_j^2$ respectively. In such a manner we can continue the observed branches of the stable stationary solutions (solid lines in Fig. 2) and draw the corresponding branches of unstable stationary solutions (dashed lines in the left part of Fig. 2).

Besides stable and unstable stationary lasing states our lasers have also other solutions. Integration of model equations for our laser at certain phase conditions have allowed to detect stable self pulsations, i.e., stable solutions with periodically oscillating carrier density and optical field power. The maximal value of the output

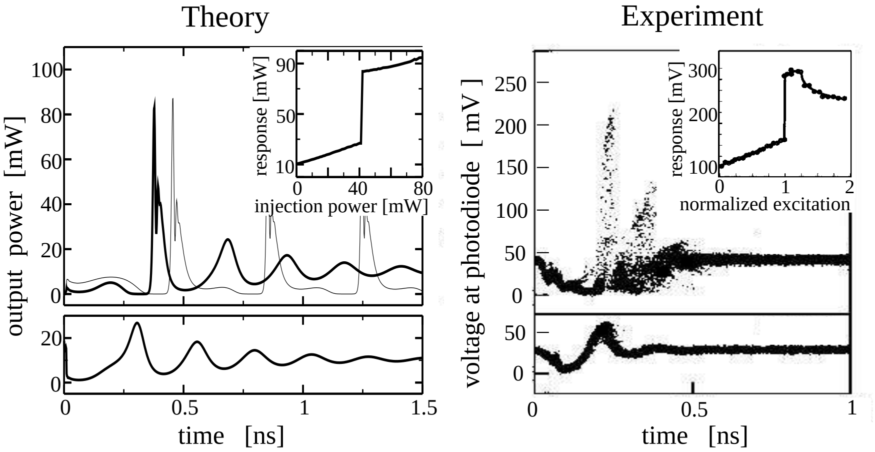

Figure 4: *Left: theoretical predictions. Right: experimental results. Upper and lower diagrams show response of the laser due to super- and sub-threshold perturbation. Thin and thick lines in the upper left diagram are due to perturbation of stationary state at different phase conditions. Sampling technique was used drawing experimental diagrams. The inserts show nonlinear response function of laser due to perturbations of different strength.*

field power at the left facet of these self pulsating solutions are indicated by the thick solid lines giving the border of intensively shadowed areas in the Fig. 3 at the phase intervals $\varphi \in [A, C]$ and $\varphi \in [E, F]$. Other thick solid lines indicate output power $\bar{f}^2$ of stable stationary states, which can be found by integration of model equations and where discussed and shown already in the left part of Fig. 2.

More advanced research of the model equations (see [24]) allows to detect also a large variety of unstable non-stationary solutions, which, nevertheless, can not be accessed by direct integration of equations and are not represented in the Fig. 3.

4 Response of the laser due to injection of a short pulse

Let us consider now nonzero optical injection via the left facet of the laser. We apply a model of an injected optical pulse defined by the function $a(t)$, where $a(t) = A > 0$ if $t \in [0, 30]$ ps and $a(t) = 0$ otherwise. The wavelength of the injected signal is ~ 8 nm longer than the wavelength of lasing state. In a such manner the injected pulse gives a perturbation of the stable lasing state. We register the maximal power of the responding output signal at the same facet starting to measure this response after the input signal is fully injected into the laser.

When adjusting phase parameter at $\varphi = 0.7$ and initial conditions at the stable stationary state with higher output power (small black circle in the left part of Fig. 3) we have observed typical to excitable systems nonlinear response function (see insert at the left part of Fig. 4). Until the injected signal gives a sub-threshold perturbation, i.e., maximal power of injection do not exceed threshold level (depicted as small triangles in Fig. 3), the response of the system is a series of decaying relaxation oscillations as depicted in the lower left diagram of Fig. 4. If the injected pulse gives a super-threshold perturbation, i.e., injected pulse power exceeds threshold level, the system is responding with a large short pulse followed by relaxation oscillations (thick line in the upper left diagram of Fig. 4). As it is indicated in the insert at the left part of Fig. 4, the maximal response of the system in both sub- and super-threshold perturbation cases grows only slightly with increased strength of injection.

We have tried to find such nonlinear response perturbing stable stationary states with maximal output power at different phase conditions and have found similar nonlinear response function only in the phase interval $\varphi \in [B, D]$ (see Fig. 3). Moreover, when $\varphi \in [B, C]$, the super-threshold perturbation of stationary state causes the transition to the stable self pulsating state (thin solid line in the upper left part of Fig. 4), what contradicts to the definition of the excitable systems. Therefore, only the light shadowed phase interval $\varphi \in [C, D]$ in the left part of Fig. 3 is indicated as an excitable region.

Thin lines within this region indicate, that such a nonlinear response is more pronounced when operating at phases $\varphi \approx C$. Here threshold perturbation (thin dashed line in Fig. 3) has smallest power, sub- and super-threshold response of the laser (thin solid line in Fig. 3) have maximal difference. Therefore, in order to observe predicted excitability in experiments, one needs to adjust initial conditions at the longer wavelength stationary solution (upper diagrams of Fig. 2) and close to the phase condition C. Since it is difficult to distinguish in experiment phases C and B, we have adjusted the phase section current close to the condition B indicated in the right part of Fig. 2.

After adjusting these conditions, we have injected into our experimental laser a 35 ps length optical pulse sequence with 15 MHz repetition frequency which have determined a sampling period (for details see [13]). The resulting sampled measured super- and sub-threshold responses of the laser and nonlinear response function are depicted in the right part of Fig. 4 showing nice agreement with theoretical predictions shown in the left part of the same figure.

5 Mode analysis of the responding signal

From now we shall analyse the contribution of different modes in the non-stationary solution $(\psi(z,t), p(z,t), n(t))$ of model equations (1). For this reason we decompose optical field and polarisation:

$$\begin{pmatrix} \psi(t) \\ p(t) \end{pmatrix} = \sum_{j=1}^{\infty} f_j(t) e^{i\Re e(\Omega_j(\bar{n}))t} \Theta_j(z, n(t)). \tag{5}$$

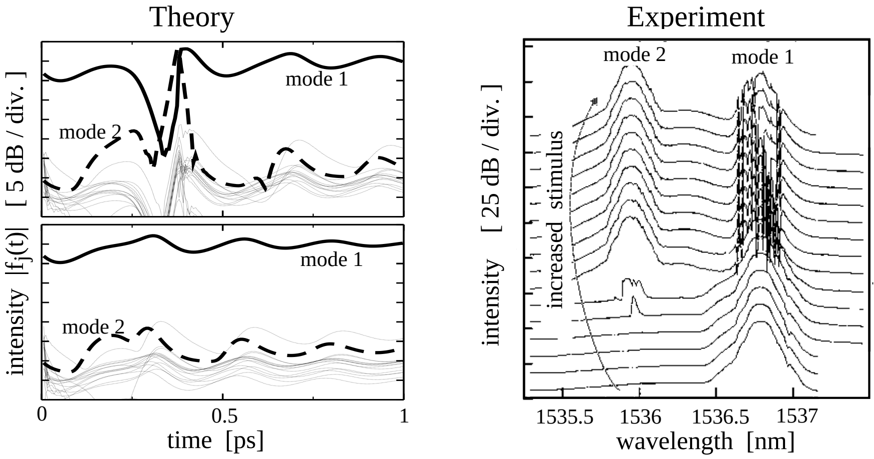

Figure 5: *Left: theoretical results. Evolution of the mode decomposition coefficients $|f_j(t)|$ when approaching stable stationary state after super-threshold (above) and sub-threshold (below) perturbation. Thick lines represent coefficients of two modes which have the main impact in the super-threshold perturbation case. Right: experimental results. A sequence of measured optical spectra for different power of injected pulse. An influence of two modes are visible in the super-threshold perturbation case.*

Here at each time moment t we use the actual value of carrier density $n(t)$ to solve the spectral equation 4 and decompose computed field and polarisation into modal components. Due to normalisation of eigenfunctions $\Theta_j(z,n)$ and due to the zero reflectivity $r_1 = 0$, complex field output at the left facet of the laser is given by expression

$$\psi^-(-L_1,t) = \sum_{j=1}^{\infty} f_j(t) e^{i\Re e(\Omega_j(\bar{n}))t}.$$

Here $f_j(t)$ are slowly varying complex amplitudes indicating contribution of corresponding mode. Fast rotation of the mode with the optical frequency $\sim \Re e(\Omega_j(\bar{n}))$ is represented by the multiplier $e^{i\Re e(\Omega_j(\bar{n}))t}$. $\bar{n}$ denotes mean value of dynamically varying $n(t)$.

Large values of $|f_j(t)|$, $j = 1,\ldots,N$ indicate N most important modes contributing to the dynamics of optical fields and polarisation. It is worth to notice, that when $N > 1$ modes contribute, the output power at the left facet is determined not only by the squared amplitude terms $|f_j(t)|^2$, but also by the nonzero mode coupling terms $\Re e(f_j^*(t) f_k(t) e^{i\Re e(\Omega_k(\bar{n})-\Omega_j(\bar{n}))t})$.

We have checked, that for our laser configuration few (one or two) terms of the mode decomposition (5) give sufficiently good approximation of the field and polarisation. The approximation error mainly depends not on the number of modes, but on the numerical precision which was used to integrate the model equations (1).

Let us investigate now in more details observed excitability depicted in the left part of Fig. 4. The injection of the short ($\delta t = 30$ ps) optical pulse starting at the time t_{inj} causes the perturbation of the operating state $(\psi(z,t_{inj}), p(z,t_{inj}), n(t_{inj}))$ of the laser. After the optical signal is fully injected into the laser (at the time moment $t_0 = t_{inj} + \delta t$), we have again an autonomous system (1) with $a(t) = 0,\ t > t_0$ and some initial conditions $(\psi(z,t_0), p(z,t_0), n(t_0))$. The behaviour of the solution before approaching again stable stationary state strongly depends on the conditions at the moment t_0.

Starting from the moment t_0 we integrate the model equations (1) at the same time decomposing computed optical field and polarisation into modal components as in (5). The values of $|f_j(t)|$ obtained in the super- and sub-threshold perturbation cases are depicted in the left part of the Fig. 4. Note the logarithmic scale of the ordinate axis in these diagrams.

Upper diagram represent super-threshold case and clearly shows the large contribution of two modes (thick lines) at certain time intervals. One can see, that the maximum of the response due to super-threshold perturbation (upper thin solid line in the Fig. 3) is due to the peak of $|f_2(t)|$. Outside the short time interval where $|f_2(t)|$ has a large peak, the second mode is suppressed and only the first mode has sufficient power.

Lower diagram indicates sub-threshold perturbation. It is clearly seen in this figure, that for all time moments only the first mode contributes and all other modes are suppressed. The second mode has no peak any more. Therefore, the maximum of the response due to the sub-threshold perturbation (lower thin solid line in the Fig. 3) is determined by the maximum of $|f_1(t)|$.

In a such manner we have demonstrated, that only two modes (if perturbation is larger) or single mode (if perturbation is smaller) determine the evolution and stabilisation of field in our laser. Indeed, the influence of two modes in the response to injected optical pulse is also clearly seen in the experiments (see right part of Fig. 5). Optical spectra of the output signal shows dominant single mode until perturbation is small and impact of two modes when perturbation exceeds threshold. The first longer wavelength mode determines stable stationary lasing state which we are trying to excite (see also upper right diagram of Fig. 2). When the perturbation is big enough, the second shorter wavelength mode also comes up and courses peaks of the responding signal (see upper right diagram of Fig. 4).

In the following section we shall consider the mechanisms of presented excitability in more details.

6 Phase portrait of the excitable system

In general the phase space of our model (1) is infinite dimensional. Nevertheless, as it was discussed in the previous section, dynamics of optical fields, polarisation functions and carrier density can be properly described by the function $n(t)$ and one or two complex amplitude functions $|f_1(t)|$ and $|f_2(t)|$ (see left part of Fig. 4).

Now the mechanism of excitability can be easily explained by the Fig. 6, where

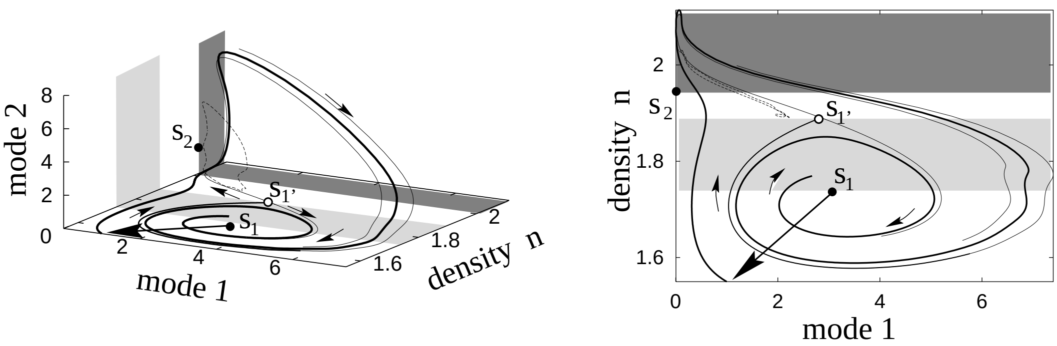

Figure 6: *Projections of the phase space of the excitable system at* $\varphi = 0.7$ *onto three- or two-dimensional subspace.*

suitable projections of two stable and saddle type stationary states (solid and empty big points), unstable limit cycle (thin dashed curve), already broken homoclinic loop (thin solid trajectories incomming and outgoing from the saddle) and a trajectory of responding signal (thick solid curve) are presented. In these figures intensively and light shaded areas indicate carrier densities supporting growth of the first or the second mode, respectively.

The system is operating at the stable stationary state s_1. The perturbation caused by injected pulse is acting along the thick arrow. If the perturbation is small, the field-density conditions remain close to the stationary state s_1 and after some decaying oscillations return back to this state.

In the case, when perturbation is strong enough, the field-density conditions can be kicked to the left side from the trajectory incomming into the saddle (solid line of medium thickness) which indicates part of the stable manifold of the saddle and defines threshold perturbation. The response trajectory makes a large excursion in the phase space bypassing the saddle stationary state $s_{1'}$ from the left and entering the intensively shaded region where the second mode becomes dominant. After returning to the plane where the first mode dominates (light shaded part and below in the right part of Fig. 6), the trajectory is attracted by the state s_1.

Such topology of the phase space is typical to the parameter region where excitability can be observed (lightly shadowed interval in the Fig. 3). When operating close to the phase parameter $\varphi = D$, the incomming into the saddle trajectory is more distant from the state s_1, thus, a threshold perturbation should be much stronger. Moreover, the excursion of the super-threshold response trajectory towards larger values of $|f_2|$, which determines a maximal super-threshold response of the system (upper thin solid line in the Fig. 3) is less pronounced in this case. The maximum of $|f_2(t)|$ becomes comparable with the maximal value of $|f_1(t)|$, which, in general, determines the maximal sub-threshold response of the system, indicated by the lower thin solid line in the Fig. 3. Therefore, when using smaller phase parameter value $\varphi < D$, for any perturbation the maximal response of the system is determined by the peak value of $|f_1(t)|$ and nonlinear response function as in the inserts of the right part of Fig. 4 will not be observed.

In the case, when we are approaching the phase parameter $\varphi \to C$, the incoming into the saddle and outgoing from the saddle trajectories come closer to each other and coincide at $\varphi = C$ forming a homoclinic connection. When further increasing parameter φ, the homoclinic connection breaks and a stable limit cycle is formed. The stable stationary state s_1 can be excited in this case as well, but instead of returning to the stationary state s_1 the trajectory of the response is attracted by this stable limit cycle. In this case the switching to the stable self pulsating solution can be observed (see thin line in the upper left diagram of Fig. 4).

7 Conclusion

We have demonstrated theoretically and experimentally how DFB laser with integrated passive phase tuning section can perform an excitable behaviour. The integration of Travelling Wave model and its mode analysis have allowed to predict excitable behaviour, to explain its origin and to select suitable operation conditions in order to demonstrate excitability in the experimental device.

Acknoledgments: We would like to thank the members of the Dynamical System group from Weierstrass Institute for Applied Analysis and Stochastics, Berlin for valuable discussions, which have allowed to understand the importance of homoclinic bifurcation. We thank also to Sebastian Wieczorek from the Free University of Amsterdam for the discussion about multi-pulse excitability in the models describing dynamics of the laser systems.

References

[1] R. FitzHugh, "Mathematical Models of Threshold Phenomena in the Nerve Membrane", *Bulletine of Mathematical Biophysics*, 17:257-278, 1955.

[2] J. Rinzel, G. B. Ermentrout, "Analysis of Neural Excitability and Oscillations", in *Methods in Neuronal Modeling*, C. Koch , I. Segev (eds), The MIT Press, Cambridge, Mass, 1989.

[3] J. D. Murray, *Mathematical Biology*, Springer 1990.

[4] S. Grill, V. S. Zykov, S. C. Müller, "Spiral wave dynamics under pulsatory modulation of excitability", *J. Phys. Chem.* **100** 19082, 1996.

[5] G. M. Shepherd, *Neurobiology*, Oxford University Press, New York, 1983.

[6] E. M. Izhikevich, “Neural Excitability, Spiking, and Bursting”, *International Journal of Bifurcation and Chaos*, 10:1171-1266, 2000.

[7] Weiping Lu, Dejin Yu, R. G. Harrison, “ Excitability in a nonlinear optical cavity”, *Phys. Rev. A* **58(2)**, pp. R809-R811, 1998.

[8] J. L. A. Dubbeldam, B. Krauskopf, D. Lenstra, “Excitability and coherence resonance in laser with saturable absorber”, *Physical Review E* **60(6)**, pp. 6580-6588, 1999.

[9] J. Mulet, C. R. Mirasso, “ Numerical statistics of power dropouts based on the Lang-Kobayashi model”, *Phys. Rev E* **59(5)**, pp. 5400-5405, 1999.

[10] M.C. Eguia, G.B. Mindlin, “Semiconductor laser with optical feedback: from excitable to deterministic low-frequency fluctuations”, *Phys. Rev. E* **60**, pp. 1551-1557, 1999.

[11] S. Wieczorek, B. Krauskopf, D. Lenstra, “Multipulse excitability”, to appear in *Physical Review Letters*, February 11, 2002.

[12] V. Z. Tronciu, H.-J. Wünsche, K. R. Schneider, M. Radziunas, “Excitability of lasers with integrated dispersive reflector”, *Proc. SPIE* **4283**, pp. 347-354, 2001.

[13] H.-J. Wünsche, O. Brox, M. Radziunas, F. Henneberger *Excitability of a semiconductor laser by a two-mode homoclinic bifurcation*, Phys. Rev. Lett., **88(2)**, pp. 23901, 2002.

[14] M. Giudici, C. Green, G. Giacomelli, U. Nespolo, J. R. Tredicce, “Andronov bifurcation and excitability in semiconductor lasers with optical feedback”, *Phys. Rev. E* **55**, pp. 6414-6418, 1997.

[15] G.H.M. van Tartwijk, I. Fischer, “ Comment on ‘Andronov bifurcation and excitability in semiconductor lasers with optical feedback’ ” , *Phys. Rev. E* **58**, pp. 4041, 1998.

[16] M. Giudici, C. Green, G. Giacomelli, U. Nespolo, J. R. Tredicce, “Reply to “Comment on ‘Andronov bifurcation and excitability in semiconductor lasers with optical feedback’ ” ”, *Phys. Rev. E* **58**, pp. 4043, 1998.

[17] J. Hales, A. Zhukov, R. Roy, et al., “Dynamics of activated escape and its observation in a semiconductor laser”, *Phys. Rev. Lett.* **85**, pp. 78-81, 2000.

[18] E. A. Viktorov, P. Mandel, “Low frequency fluctuations in a multimode semiconductor laser with optical feedback”, *Phys. Rev. Lett.* **85**, pp. 3157, 2000.

[19] U. Bandelow, M. Radziunas, J. Sieber, M. Wolfrum, “Impact of Gain Dispersion on the Spatio-Temporal Dynamics of Multisection Lasers”, *IEEE J. Quantum Electron.* **37**, pp. 183-188, 2001.

[20] U. Bandelow, H.-J. Wünsche, B. Sartorius, M. Möhrle, "Dispersive self Q-switching in DFB-lasers: theory versus experiment", *IEEE J. Selected Topics in Quantum Electron.* **3**, pp. 270-277, 1997.

[21] M. Radziunas, H.-J. Wünsche, B. Sartorius, O. Brox, D. Hoffmann, K. Schneider, D. Marcenac, "Modeling self-pulsating DFB lasers with integrated phase tuning section", *IEEE J. Quantum Electron.*, **36**, pp. 1026-1034, 2000.

[22] A.A. Tager, K. Petermann, "High-frequency oscilations and self-mode locking in short external-cavity diodes", *IEEE J. Quantum Electron.* **30**, pp. 1553, 1994.

[23] H. Wenzel, U. Bandelow, H.-J. Wünsche, J. Rehberg, "Mechanisms of fast self pulsations in two-section DFB lasers", *IEEE J. Quantum Electron.*, **32**, pp. 69-78, 1996.

[24] J. Sieber, "Numerical bifurcation analysis for multi-section semiconductor lasers", *WIAS Preprint* (Weierstrass Institute of Applied Analysis abd Stochastics, Berlin), **683**, 2001.